J. Fluid Mech. (1996), *vol.* 319, *pp.* 125–149

Helicity generation and vorticity dynamics in helically symmetric flow

By MASANORI TAKAOKA†

Department of Mechanical Engineering, Faculty of Engineering Science, Osaka University, Toyonaka, Osaka 560, Japan

(Received 21 March 1995 and in revised form 1 March 1996)

Helicity generation and vorticity dynamics in a helically symmetric flow are studied numerically by solving the Navier–Stokes equations in an unbounded domain. The helical symmetry reduces the problem to one in two dimensions, which makes it practicable to use an analytical expression for vortex surfaces. Furthermore, the field still retains three-dimensional aspects, such as helicity and vortex stretching. To every vortex surface there corresponds an inviscid invariant of helicity.

Our initial conditions are chosen as two cases of twisted elliptical tubes of high vorticity. The first case has elliptical vortex surfaces, which is a helically symmetric version of the initial condition employed by Aref & Zawadzki (1991), but the second case has axisymmetric vortex surfaces. The total helicity inside every vortex surface is zero in both the initial fields. It is found that vortex stretching plays an important role in the time evolution of the first case, but not of the second case.

We examine the relation of the vorticity dynamics to the helicity generation by using the representation of the vortex lines and the vortex surfaces rather than the equi-vorticity surfaces. This leads to new concepts for the mechanisms of formation of the spiral vortex structures observed for the two cases. The detailed investigation of the helicity generation is done by examining the distribution of the helicity on each vortex surface and the Fourier spectrum of helicity. The processes of helicity generation due to the vortex stretching are different for each initial condition. The viscosity dependence of 'inviscid' invariants shows that with smaller viscosity, only in the first case is more helicity generated. This is because in the first case where there is vortex stretching the contact zones of the adjacent vortex layers are elongated and the local vorticity is intensified to an extent limited by viscosity. Thus with smaller viscosity a more intense vortex is reconnected to generate more helicity. As expected, in both cases more of the energy is preserved with smaller viscosity.

1. Introduction

Both helicity and vortex stretching are inherent properties of three-dimensional flows, and play fundamental roles in turbulence theory. In order to know which is the best cascade theory, it is important to examine which of the two inviscid conserved quantities, the kinetic energy or the helicity, is more dissipated in a slightly viscous case. The competition between vortex stretching and viscous dissipation is crucial in the singularity problem of a solution to the three-dimensional Navier–Stokes equation.

† Present address: Division of Physics and Astronomy, Graduate School of Science, Kyoto University, Kyoto 606-01, Japan.

A helically symmetric flow is one of the simplest flows possessing these characteristics, although it depends only on two space variables. Such a flow in a circular pipe has already been investigated extensively both theoretically and numerically by many researchers (Kelvin 1880; Landman 1990*a*,*b*; Dritschel 1991 and references therein). In the present paper, we numerically simulate a helically symmetric flow in an unbounded domain, which may remove inessential complexity due to the interaction with the boundary when we consider the generation mechanism of helicity. No singularity is expected in either two-dimensional or cylindrically symmetric flows because there is no vortex stretching. Another of the simplest systems with vortex stretching is a rotationally symmetric flow, that is an axisymmetric flow with swirl. Using the rotationally symmetric flow, the generation of finite time singularities in an Euler flow was investigated numerically (Grauer & Sideris 1991; Pumir & Siggia 1992). We know the mathematical result that in a circular pipe no singularity will appear in the Navier–Stokes flow with helical symmetry (Mahalov, Titi & Leibovich 1990). The singularity problem of the Euler equation with the present symmetry will be reported elsewhere.

The preservation property of kinetic energy and helicity, both of which are quadratic in the velocity, in an inviscid fluid may restrict the dynamics of a large-length-scale and/or high-Reynolds-number flow. Note that in contrast with the kinetic energy, not only the total helicity but also every patch of helicity surrounded by any vortex surface† are inviscid conserved quantities. The helicity for each vortex surface is, of course, Galilean invariant, which is in contrast to the non-Galilean invariance of helicity density. And helicity is clearly related to the topology of vortex filaments, knottedness and circulation (Moffatt 1969; Moffatt & Ricca 1992; Moffatt & Tsinober 1992; Tur & Yanovsky 1993). Also, helicity has been referred in the discussion of vorticity reconnection (Kida & Takaoka 1987, 1988). It is desirable to use vortex surfaces in the study of phenomena related to helicity, though equi-vorticity surfaces, high-vorticity regions, have been used in most numerical simulations of vorticity dynamics. Differences between vortex surfaces and equi-vorticity surfaces are enlarged by the effect of vortex stretching (Kida & Takaoka 1991, Takaoka 1991). Although constructing the vortex surface is difficult in a general three-dimensional flow, the present symmetry makes it practicable as an explicit form (see § 2).

The helicity may increase or decrease depending on the sense of its skewed structure, which is a contrast to the monotonic decrease of kinetic energy. It is known that some non-Galilean-invariant forcing to small-length-scale motions can generate a large-length-scale structure with non-zero helicity in a turbulent flow (Krause & Rudiger 1974; Frisch, She & Sulem 1987). This is called the AKA-effect, and is formally similar to the α-effect for a magnetic field. This breaking of the Galilean invariance is closely related to the lack of reflectional symmetry (see for example Moffatt & Tsinober 1992). A velocity field with non-zero helicity lacks reflectional symmetry. But the lack of reflectional symmetry does not necessarily mean that the field will have non-zero helicity. In a numerical simulation of a collision of two unlinked elliptical rings of high vorticity, which are set to be without reflectional symmetry or helicity, Aref & Zawadzki (1991) demonstrated the generation of linkage of vortex tubes and therefore of helicity. The helicity, or the linkage and the knottedness of

† We use this word for the surface of a vortex tube. In the present paper, a 'vortex tube' is used for a bundle of vortex lines, whose tangent at any point is in the direction of the vorticity field, though the word 'vortex' has sometimes been used for the localized high-vorticity region.

vortex lines, is generated through vorticity reconnection, but the reverse is not always the case (Kida & Takaoka 1987, 1988, 1994; Kida, Takaoka & Hussain 1991).

In the present paper, our main purpose is a detailed investigation of such helicity generation by using a helically symmetric flow. Reducing the dimensions by one, we are able to simulate a flow with a much larger Reynolds number, which enables us to investigate the Reynolds number dependence and to conjecture the behaviour in an inviscid limit.

This paper is organized as follows. In § 2, we introduce some notation and derive basic equations which govern a helically symmetric flow in an unbounded domain. The field is determined by two scalar functions (ψ and χ) of two space variables (r and ϕ). In § 3, our numerical method is briefly explained. Initial conditions reported here have zero total helicity with large vortex structure, in order to focus our attention on the generation of helicity and its relation with vorticity dynamics. One of our initial fields can be considered as the continuous version of the flow investigated by Aref & Zawadzki (1991). Numerical results for this initial condition are collected in § 4. Another initial condition, having the same equi-vorticity surface but a different vortex structure, is also examined and compared briefly in § 5. And the last section is devoted to concluding remarks.

2. Formulation for a helically symmetric flow

We say that a vector field $\boldsymbol{v}$ has helical symmetry when it can be expressed in cylindrical polar coordinates (r, θ, z) as

$$\boldsymbol{v} = \boldsymbol{v}(r, \phi, t)\,, \tag{2.1}$$

where $\phi = \theta + \epsilon z$, and ϵ is a parameter representing the pitch in the z-direction as $(2\pi/\epsilon)$ (Landman 1990*a*). It should be noted that this does not mean that the vortex lines and the stream lines have helical structure with the same pitch. It is convenient to introduce a Beltrami vector to represent this flow (Dritschel 1991):

$$\boldsymbol{h} = h^2(\boldsymbol{e}_z - \epsilon r \boldsymbol{e}_\theta)\,, \tag{2.2}$$

and

$$h^2 = \frac{1}{1 + \epsilon^2 r^2}. \tag{2.3}$$

Note that the Beltrami vector is not a unit vector. Furthermore it has following properties:

$$\nabla \cdot \boldsymbol{h} = 0, \quad \nabla \times \boldsymbol{h} = -2\epsilon h^2 \boldsymbol{h}, \quad \boldsymbol{h} \cdot \nabla f(r, \phi, t) = 0, \tag{2.4}$$

where f is an arbitrary function. The last equation is another expression of the helical symmetry.

Let us introduce two scalar functions $\psi(r, \phi, t)$ and $\chi(r, \phi, t)$. The velocity $\boldsymbol{u}$ of the incompressible fluid and its curl, vorticity $\boldsymbol{\omega}$, may be written as

$$\boldsymbol{u} = -\boldsymbol{h} \times \nabla\psi - \boldsymbol{h}\chi, \quad \boldsymbol{\omega} = \boldsymbol{h} \times \nabla\chi + \boldsymbol{h}(2\epsilon h^2 \chi + \varpi)\,, \tag{2.5}$$

where

$$\varpi = -\Delta^\star \psi, \ \nabla = \boldsymbol{e}_r \frac{\partial}{\partial r} + \boldsymbol{e}_\phi \frac{1}{rh} \frac{\partial}{\partial \phi}, \ \text{and } \Delta^\star = \frac{1}{rh^2} \frac{\partial}{\partial r}\left(rh^2 \frac{\partial}{\partial r}\right) + \frac{1}{r^2 h^2} \frac{\partial^2}{\partial \phi^2}.$$

It is worth noting that from (2.5) one knows $\nabla\chi \cdot \boldsymbol{\omega} = 0$ and $\nabla\psi \cdot \boldsymbol{u} = 0$, which means that the level surfaces of an arbitrary function of χ and ψ are vortex surfaces and

stream sheets, respectively. When $\chi \equiv 0$ (or $\psi \equiv 0$), cylindrical surfaces (r =const.) are the vortex surfaces (or stream sheets).

2.1. *Governing equations*

We next derive governing equations for ψ and χ, which describe a flow having the present symmetry. The basic equations of an incompressible fluid motion are composed of the Navier–Stokes equation and the continuity equation. The latter equation is already satisfied by virtue of (2.5). Putting these expressions into the vorticity equation, the curl of the Navier–Stokes equation, we obtain a set of equations to determine the time-evolution of ψ and χ :

$$\frac{\partial \chi}{\partial t} = \frac{1}{r}\frac{\partial(\psi, \chi)}{\partial(r, \phi)} + \nu\Delta^*\chi - 4\nu\epsilon^2 h^4\chi + 2\nu\epsilon h^2\Delta^*\psi, \tag{2.6}$$

$$\frac{\partial \varpi}{\partial t} = \frac{1}{rh^2}\frac{\partial(\psi, h^2\varpi)}{\partial(r, \phi)} + \frac{2\epsilon h^2}{r}\frac{\partial(\psi, \chi)}{\partial(r, \phi)} - 2\epsilon^2 h^2\chi\frac{\partial \chi}{\partial \phi} + 8\epsilon^3 h^4\chi\frac{\partial \psi}{\partial \phi} + 2\nu\epsilon\Delta^*(h^2\chi) + \nu\Delta^*\varpi, \tag{2.7}$$

$$\varpi = -\Delta^*\psi, \tag{2.8}$$

where use has been made of equations (2.4).

In the case of $\epsilon = 0$, equation (2.7) is reduced to the two-dimensional vorticity equation expressed in terms of the stream function $\psi(r, \theta, t)$, and equation (2.6) becomes the governing equation for the passive scalar field $\chi(r, \theta, t)$ advected by the same velocity with the same diffusivity in the two-dimensional flow. In the limit $\epsilon \to \infty$, on the other hand, in the rescaled variables $\tilde{\chi} = \chi/\epsilon$ and $\tilde{\psi} = \psi/\epsilon$, they are reduced to the equation of motion for an axisymmetric flow expressed in terms of the Stokes' stream function $\tilde{\psi}(r, z, t)$.

For convenience in the later discussion, we define here several integrated physical quantities, such as energy E, enstrophy Q, helicity H, and rate of helicity change $\mathrm{d}H/\mathrm{d}t$, in terms of ψ and χ as follows:

$$E = \frac{1}{2}\int\int \{\psi\varpi + \chi^2\}\, h^2 r \mathrm{d}r\mathrm{d}\phi, \tag{2.9}$$

$$Q = \frac{1}{2}\int\int \{(\nabla\chi)^2 + (\varpi + 2\epsilon h^2\chi)^2\}\, h^2 r \mathrm{d}r\mathrm{d}\phi, \tag{2.10}$$

$$H = -2\int\int \{\varpi + \epsilon h^2\chi\}\, \chi h^2 r \mathrm{d}r\mathrm{d}\phi, \tag{2.11}$$

$$\frac{\mathrm{d}H}{\mathrm{d}t} = 4\nu\int\int \left[\{\epsilon h^2(\varpi + 2\epsilon h^2\chi) - \Delta^*\chi\}\,(\varpi + 2\epsilon h^2\chi)\right] h^2 r \mathrm{d}r\mathrm{d}\phi. \tag{2.12}$$

In a two-dimensional flow, when the total circulation of the component of vorticity perpendicular to the plane is not zero, the total energy $E_0 = \frac{1}{2}\int |\boldsymbol{u}|^2 r \mathrm{d}r\mathrm{d}\phi$ is infinite because of the logarithmic dependence on r of the primitive function, even if the vorticity decreases in space sufficiently fast. To avoid this problem of infinity, use has been made of partial integration in the above definition of energy. The time variation of E and E_0 is the same, the difference is just the infinitely large constant.

3. Numerical method and initial conditions

3.1. *Numerical method*

In order to solve equations (2.6) and (2.7) numerically, the Fourier expansion in the ϕ-direction is employed on ψ and χ as

$$\psi(r,\phi,t) = \sum_{n=-N_\phi/3}^{N_\phi/3} \psi_n(r,t)\,\mathrm{e}^{in\phi}\,, \quad \chi(r,\phi,t) = \sum_{n=-N_\phi/3}^{N_\phi/3} \chi_n(r,t)\,\mathrm{e}^{in\phi}, \tag{3.1}$$

where $\psi_{-n} = \psi_n^*$, $\chi_{-n} = \chi_n^*$ and $*$ denotes the complex conjugate. A pseudo-spectral method with an N_ϕ-mode fast Fourier transformation is used in the evaluation of the ϕ-direction and the aliasing errors appearing in the evaluation of the nonlinear terms are removed by the 2/3-law. We further introduce a new independent variable ξ to map a semi-infinite region $0 \leqslant r < \infty$ onto a finite region $0 \leqslant \xi < 1/2$, where ξ is defined as $r = R_0\tan(\pi\xi)$. R_0 is an adjustable parameter and we set $R_0 = 3$ in the present simulation. In the radial ξ (r)-direction, a second-order central finite difference scheme is used. We divide the space in the ξ-direction into N_r equal-size meshes so that the size of a radial grid in r-space is $\pi R_0/2N_r\,(1 + r^2/R_0^2)$. It is expected in our simulation that for large r both χ and $\varpi = -\Delta^*\psi$ decay exponentially fast and the characteristic scales also increase.

The function ψ is obtained by solving the Poisson equation (2.8) which is now separated for each Fourier mode as

$$-\left\{\frac{1}{rh^2}\frac{\partial}{\partial r}\left(rh^2\frac{\partial}{\partial r}\right) - \frac{n^2}{r^2h^2}\right\}\psi_n = \varpi_n. \tag{3.2}$$

For n $\geqslant 1$, the Laplace operator on the left-hand-side of (3.2) is expressed by a band matrix in terms of the finite difference scheme and solved inversely to obtain ψ_n by the Gauss elimination method. When $n = 0$, this Poisson equation is

$$-\frac{1}{rh^2}\frac{\mathrm{d}}{\mathrm{d}r}\left(rh^2\frac{\mathrm{d}\psi_0}{\mathrm{d}r}\right) = \varpi_0. \tag{3.3}$$

If $\Gamma_z = \int \varpi_0 rh^2\mathrm{d}r \neq 0$, ψ_0 may diverge as $r \to \infty$, irrespective of how fast ϖ_0 itself decays. Fortunately, however, we do not have to use ψ_0 itself in our simulation since we can rewrite the basic equations in terms of $h^2\mathrm{d}\psi_0/\mathrm{d}r$, which may decay to zero even if Γ_z is finite. Formally we perform the integration

$$h^2\frac{\mathrm{d}\psi_0}{\mathrm{d}r} = -\frac{1}{r}\int_0^r sh^2(s)\varpi_0(s)\mathrm{d}s \tag{3.4}$$

in ξ-space (see also Buntine & Pullin 1989).

In the time integration we use a modified Runge–Kutta–Gill scheme, and some of the viscous terms, which are linear and do not depend on the space variables explicitly, are analytically integrated and included in the modified scheme to stabilize it (see also Landman 1990*a*). In the following simulation, different numbers of grids and modes (N_r, N_ϕ) are used depending on the Reynolds number (see table 1). Two simulations, run-3d and run-5d, have been done to check the numerical accuracy.

3.2. *Initial conditions*

Two types of initial conditions are adopted to examine helicity generation. Our initial condition for the first case, Case I, is the following one, which is a helically symmetric

Run	$N_r \times N_\phi$	ν	Final time
run-1	128×64	0.005	20
run-2	128×64	0.002	30
run-3	128×64	0.001	40
run-3d	256×128	0.001	40
run-4	256×128	0.0005	50
run-5	256×128	0.0002	50
run-5d	512×256	0.0002	50
run-6	512×256	0.0001	50

TABLE 1. Parameters used in the simulations of Case I.

version of the initial condition employed by Aref & Zawadzki (1991):

$$\chi = \exp\left\{-r^{2p}\left(\frac{\cos^2\phi}{a^2} + \frac{\sin^2\phi}{b^2}\right)^p\right\}, \tag{3.5}$$

$$\varpi = -2\epsilon h^2 \chi - \epsilon r \frac{\partial \chi}{\partial r} = 2\epsilon\left\{pr^{2p}\left(\frac{\cos^2\phi}{a^2} + \frac{\sin^2\phi}{b^2}\right)^p - h^2\right\}\chi, \tag{3.6}$$

where ϵ, p, a and b are free parameters. The functional form of (3.5) is chosen so as to have an elliptical ring structure with an equi-vorticity surface on a z-constant cross-section. The condition (3.6) is determined for the vorticity field to be two-dimensional, i.e. $\omega_z = 0$ everywhere. Every vortex line is then initially unlinked, which means the total helicity is zero. After some algebra, we find that the rate of helicity change is also zero at the initial instance.

The other initial condition, Case II, is

$$\chi = 0, \tag{3.7}$$

$$\varpi = \frac{2pr^{2p-1}}{h}\left(\frac{\cos^2\phi}{a^2} + \frac{\sin^2\phi}{b^2}\right)^{p-1} \exp\left\{-r^{2p}\left(\frac{\cos^2\phi}{a^2} + \frac{\sin^2\phi}{b^2}\right)^p\right\} \times \left\{\left(\frac{\cos^2\phi}{a^2} + \frac{\sin^2\phi}{b^2}\right)^2 + \sin^2\phi\cos^2\phi\left(\frac{1}{a^2} - \frac{1}{b^2}\right)^2\right\}^{1/2}, \tag{3.8}$$

whose equi-vorticity surfaces are the same as those in Case I. Equation (3.7) makes the helicity density $\boldsymbol{u}\cdot\boldsymbol{\omega}$ zero everywhere as well as the total helicity. The rate of helicity change, on the other hand, is not zero from the start. As we will see in later discussion, the role of vortex stretching is an essential difference between the two cases.

We will report, in the following, the results for the case of $\epsilon = 1$, $p = 2$, $a = 3$ and $b = 1$. Note here that (2.6) and (2.7) are invariant under the transformations $(\psi, \phi, \epsilon) \to (-\psi, -\phi, -\epsilon)$ or $(\chi, \psi, \phi) \to (-\chi, -\psi, -\phi)$. Then, if $\epsilon_1 = -\epsilon_2$, the dynamics for $\epsilon = \epsilon_1$ and $\epsilon = \epsilon_2$ are identical except for the signs of pseudo-scalars such as helicity. A perspective view of the equi-vorticity surface of the present initial field is shown in figure 1. An elliptical tube of high vorticity, which is composed of elliptical rings in the (x, y)-plane, is twisted uniformly in the z-direction. This presentation is good for surveying a three-dimensional structure, but it loses rich information, such

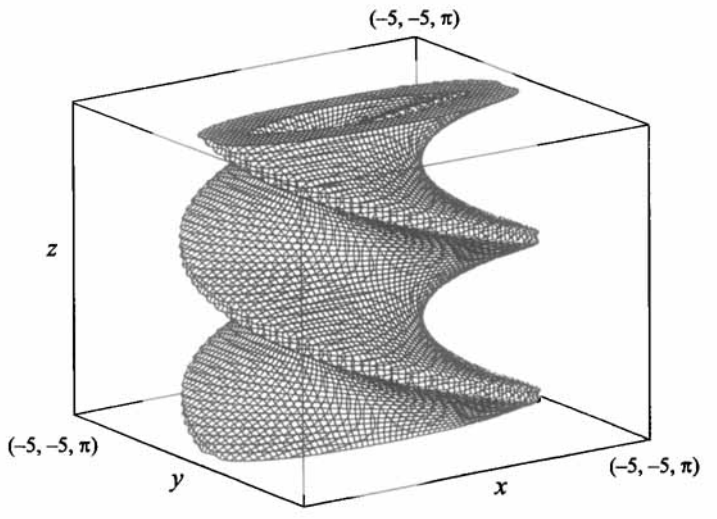

FIGURE 1. Perspective view of the equi-vorticity surface of the initial condition. Cases I and II have the same equi-vorticity surfaces, but different vortex structure, vortex surfaces and lines. It is seen from the $(2, 3, 1)$-direction, and the surface level is 50% of its maximum $\omega_{max} = 2.7$.

as the structure of vortex lines, the relation between different levels of vortex surfaces, and so on. In the following figures, we therefore use the three-dimensional view of vortex lines or the two-dimensional view of a cross-section on the (x, y)-plane. I hope readers can reconstruct three-dimensional images from these figures using their imagination.

4. Numerical results for Case I

4.1. *Vorticity dynamics*

Figure 2(*a*) shows the vortex lines at the initial instant, each of which is started on a regular grid point in the (x, y)-plane. Although we simulate the field in an unbounded domain of (x, y, z)-space, we show only a box near the origin ($x = y = 0$) for convenience of display. To clarify the three-dimensional structure of the field, we show four perspective views seen from the z-, y-, x- and $(2, 3, 1)$-directions. From the direction and the length of each vortex line drawn there, we know the direction and intensity of vorticity field.

The time-evolution of the vorticity field is shown in figure 2(*b–d*). Initially the elliptical structure is deformed into an S-shape, or a combination of two facing arcs shifted by half a unit, by the induction velocity. During the deformation, the z-component of vorticity appears and vortex lines become three-dimensional (figure 2*b*). Readers may recognize that, as a whole, the vortex lines elongated toward the origin $(x, y) = (0, 0)$, which are the concave sides of the arcs, have a positive z-component of vorticity, and the vortex lines elongated outward, which are the convex sides of the arcs, have a negative z-component of vorticity. This result is easily understood by considering the velocity field discussed later (see the last paragraph in the present subsection). The S-shape of vortex lines is stretched and deformed into a spiral structure made of thin vortex layers (figure 2*c*). The growth of enstrophy at this stage (see figure 9) suggests intense vortex stretching. Finally, an axisymmetric structure emerges from the centre, and its radius becomes larger with time through viscous

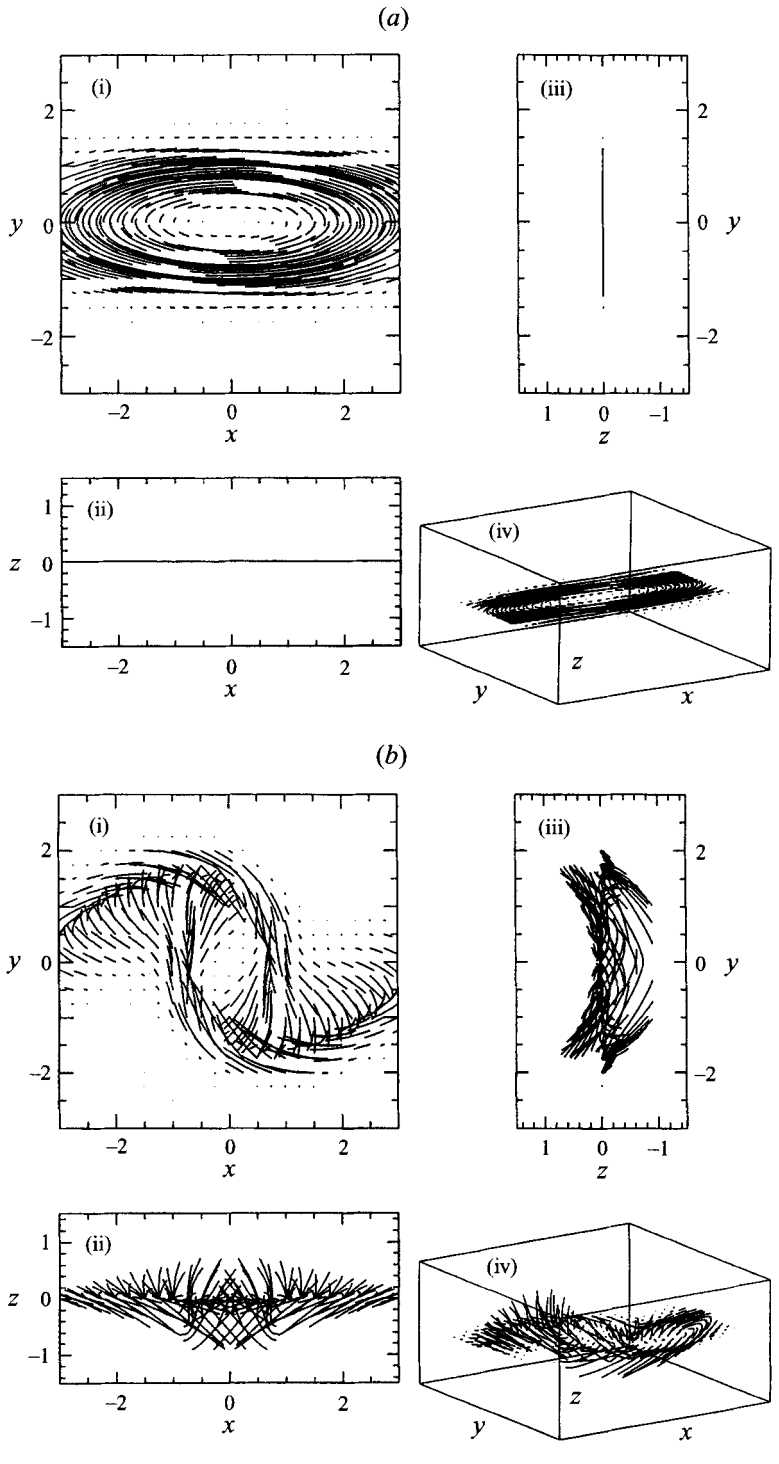

FIGURE 2 (*a*, *b*). For caption see facing page.

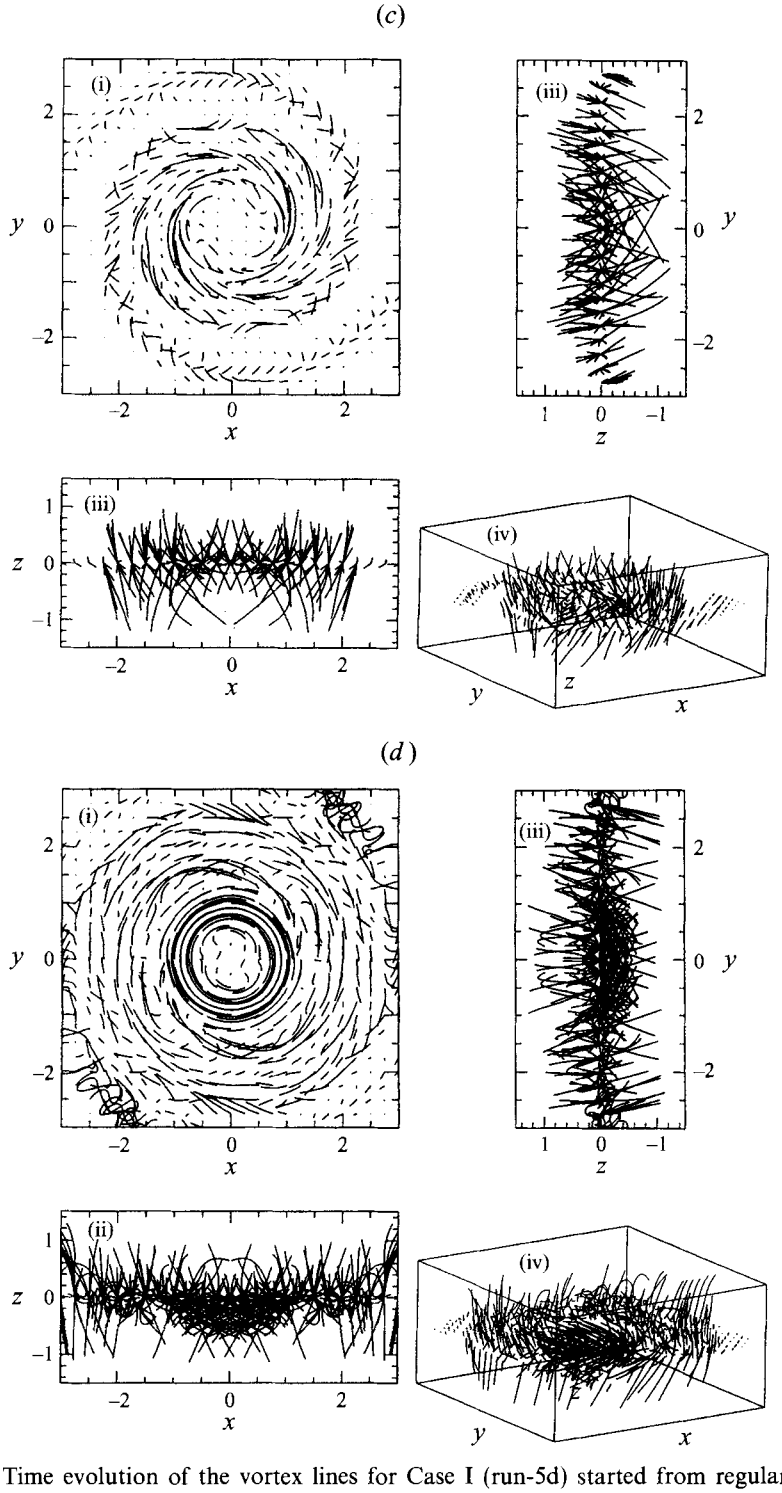

FIGURE 2. Time evolution of the vortex lines for Case I (run-5d) started from regular grid points on the (x, y)-plane, now $z = 0$. The grid size is 0.25 in each direction. They view is from the (i) z-, (ii) y-, (iii) x- and (iv) $(2, 3, 1)$-directions. (*a*) $t = 0$, (*b*) $t = 3$, (*c*) $t = 15$, (*d*) $t = 50$.

diffusion (figure 2*d*). It should be noted that the z-component of vorticity near the origin is changed from positive (figure 2*b*) to negative (figure 2*d*), which corresponds to the change of the sign of the total helicity discussed later.

Breaking of the mirror symmetry, which the initial field has in the (r, ϕ)-plane, is caused by the nonlinear effect, as seen from equations (2.6) and (2.7) by changing $\phi \to -\phi$. This symmetry breaking is observed as the generation of spiral structure and therefore of helicity. In the presentation of equi-vorticity surfaces, one is reminded of a similar process, a symmetric vortex merging, of two like-signed vortex patches in a usual two-dimensional flow (Melander, Zabusky & McWilliams 1988; Buntine & Pullin 1989). However, the dynamics involved is quite different, that is vortex stretching, directional change of vorticity, and generation of helicity. It should be noted that in our case the vorticity field is not a scalar field but a vector field, and the total circulation of ω_z is zero for all the time.

We will give a simple explanation for the generation mechanism of the spiral structure by using the Fourier expression (3.1). Let all the Fourier components for odd wavenumbers be zero, which is the case here, and the zeroth modes (ϖ_0 and χ_0) and the second ones (ϖ_2 and χ_2) be of the same order. If the typical length scale of the field ψ in the r-direction is R_ψ, then, roughly speaking, the Laplace operator magnifies the nth mode by $(1+n^2)/R_\psi^2 + n^2\epsilon^2$. Then the ratio ψ_2/ψ_0 of the typical magnitude of the zeroth and the second modes of ψ is smaller than those of ϖ and χ, i.e. ϖ_2/ϖ_0 and χ_2/χ_0. That is, $\psi(r, \phi, t)$ is more axisymmetric than $\varpi(r, \phi, t)$ and $\chi(r, \phi, t)$. This argument is supported numerically; see figure 3, where the contour plots of ψ, ϖ, and χ are drawn. Now recall that the level surfaces of ψ and χ give stream sheets and vortex surfaces, respectively, as mentioned in §2. The velocity field has a more circular structure than the vorticity field. However, one must not hastily conclude that this circular velocity makes the field spiral. Note that the azimuthal velocity is written as $u_\theta = h^2(-\partial\psi/\partial r + \epsilon r\chi)$, and the circulation of this velocity is zero: $\int_0^{2\pi} u_\theta r \mathrm{d}\theta = 0$ for all r, which is different from the well-known situation of the vortex merging in a pure two-dimensional simulation. Comparing the 'form' of the Jacobian term in the basic equations (2.6) and (2.7) with that in the usual two-dimensional Navier–Stokes equation, one might think of a 'virtual stream function' ψ. And the circulation of virtual azimuthal velocity ($v_\theta = \partial\psi/\partial r$) is non-zero: $\int_0^{2\pi} v_\theta r \mathrm{d}\theta \neq 0$, which is negative and is consistent with the direction of the spiral structure.

Another representation for this is as follows. Considering the three-dimensionality, one can understand that a rotating flow is not indispensable. The key to understanding is the velocity in the z-direction, u_z, which makes the difference between u_θ and v_θ. Let us imagine the elliptical vortex rings with different height z, as in the schematic illustration in figure 4. Since u_z is a function of r, the vorticity fields with different height are advected to the same height at a later time. Since, on the whole, downward velocity is larger for smaller radius, the thick portion of the vortex lines in figure 4, for example, will be in a common plane after some time. Thus one will see the spiral structure in the (x, y)-plane. This downward velocity and its distribution also makes the vortex lines three-dimensional as pointed out previously.

4.2. *Helicity generation*

We next look at the dynamics of the field in terms of the distribution of helicity. Helicity surrounded by vortex surfaces, not equi-vorticity surfaces, is an inviscid invariant of motion. Vortex surfaces are given explicitly by the level surfaces of an arbitrary function of $\chi(r, \phi)$ for a flow having the present symmetry. In figure 5, we

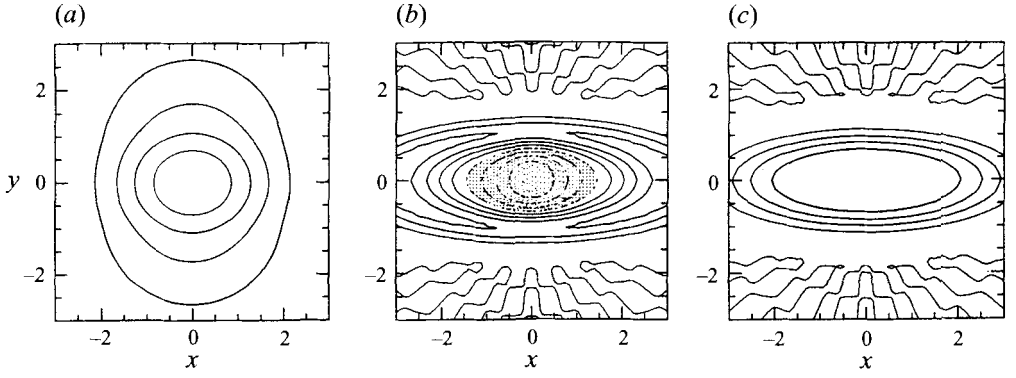

FIGURE 3. Contour plots of the fields of (*a*) ψ, (*b*) ϖ, and (*c*) χ at $t = 0$ for Case I on the (x, y)-plane. Contour lines are drawn every 20% of the maximum (or minimum) value of each field. In (*b*), dashed lines represent negative values and the shaded region shows the field having smaller value than −20%.

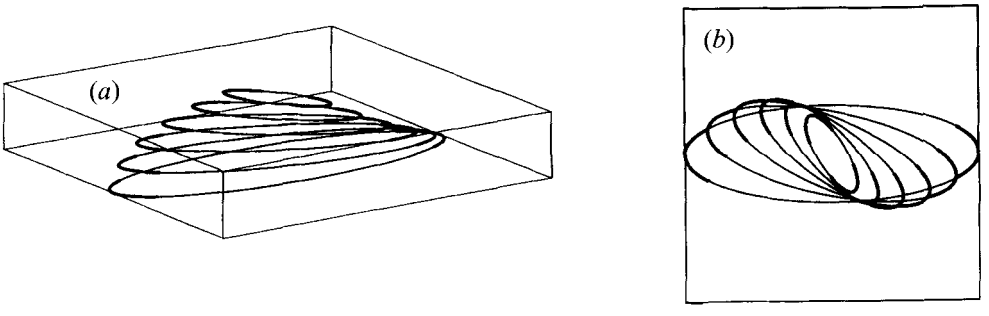

FIGURE 4. Schematic illustrations of the generation mechanism of the spiral structure: (*a*) perspective view, (*b*) projected lines on the (x, y)-plane. The thick portion of the vortex lines will be in a common plane after some time.

show the time evolution of the level surfaces of χ. For the initial field, one knows from (3.5) that χ monotonically decreases from 1 to 0 as r increases. Since χ itself is varied, diffused, by the viscous effect, we are not able to track each vortex surface exactly in time. The dynamics of vortex surfaces is almost the same as that of the vortex lines depicted in the preceding subsection. Elliptical vortex surfaces are changed to S-shape, spiral and axi-symmetric structures in order.

Although the distribution of helicity density has been examined numerically by many researchers, the value of helicity density is not Galilean invariant. However, little is known about the distribution of helicity within each vortex surface, which is Galilean invariant, because of the difficulty in constructing the vortex surface for general three-dimensional flows. We numerically calculate the density of helicity and that of the rate of helicity change in the area of $[\chi, \chi + \delta\chi]$ by integrating the helicity density $\boldsymbol{u} \cdot \boldsymbol{\omega}$ and the density of the rate of helicity change $\boldsymbol{\omega} \cdot (\nabla \times \boldsymbol{\omega})$ multiplied respectively by an area element $r dr d\phi$ and divided by the area. The distribution of the density of helicity on each vorticity surface and that of the rate of helicity change are plotted in figures 6(*a*) and 6(*b*), respectively. In the early period ($t < 10$) no localizing is observed, but broad and small distributions of negative helicity and of rate of helicity change are seen (see the lower two lines in figure 6). In the later period

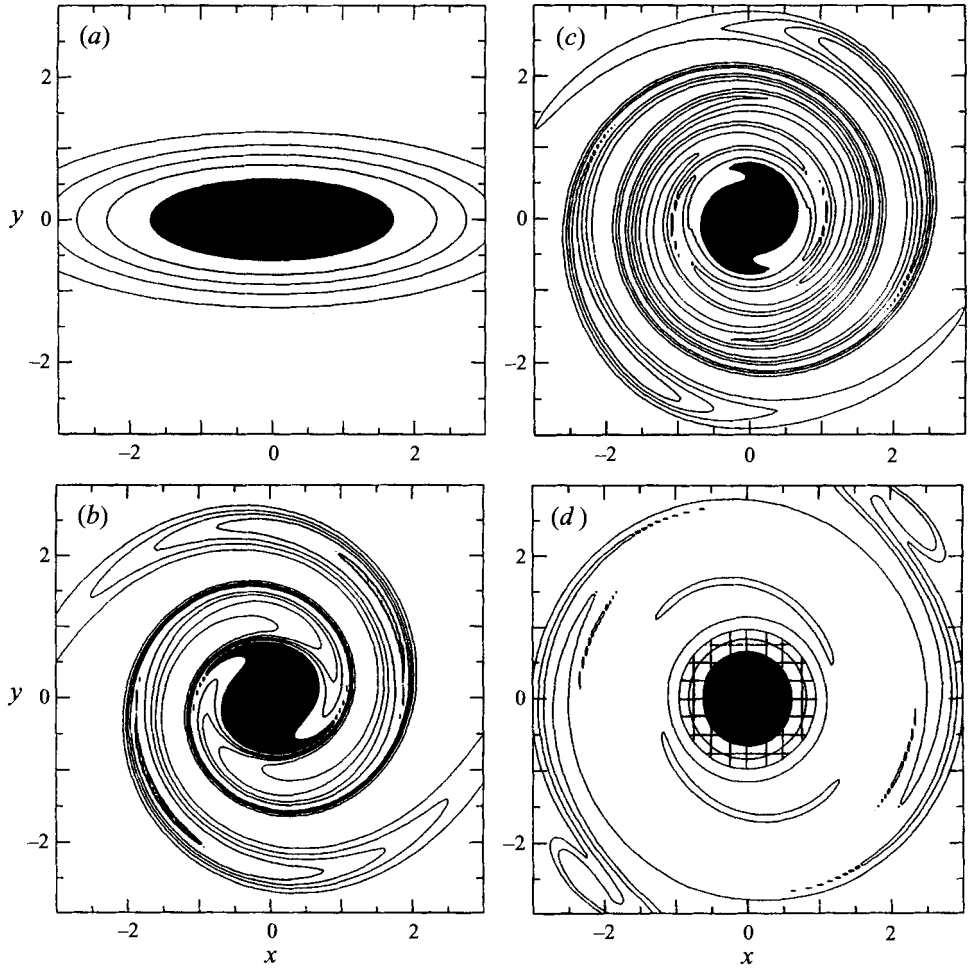

FIGURE 5. Time evolution of the vortex surfaces (the level surfaces of χ) for Case I (run-5d). Contour lines are drawn 10, 30, 50, 70, 90% of the instantaneous maximum. The region with level above 90% is shaded. (*a*) $t = 0$, (*b*) $t = 10$, (*c*) $t = 20$, (*d*) $t = 50$.

($t \geqslant 10$) positive helicity is generated from the centre and spreads out, corresponding to the growth of an axisymmetric structure of vorticity (see the upper five lines in figure 6).

Comparing figures 5 and 6(*a*, *b*), we see the relation between vortex surfaces and the distribution of helicity (that of the rate of helicity change). For example, in figure 5(*c*) at $t = 20$, we shade the region whose level is above 90% of its instantaneous maximum. The corresponding line in figure 6(*a*) takes a peak value around there, shown by the arrow†. Helicity is mostly generated on the surface of the spiral layers, where the small length scale and viscous effects dominate. In other words, vorticity reconnection occurs actively there, which is confirmed by drawing the $\nu(\Delta\omega)_\perp$-field (but those figures are omitted here) (see Kida & Takaoka 1991). Once the localized helicity is generated near the origin, its change is almost negligible. In figure 5(*d*) at $t = 50$, a grid pattern is also drawn in the region within the 50%-contour line,

† The step near the peak in figure 6(*a*) is more clearly seen when we remove the contribution from the 'two islands', at (−2.3, −2.4) and (2.3, 2.4) in figure 5(*d*), outside the spiral.

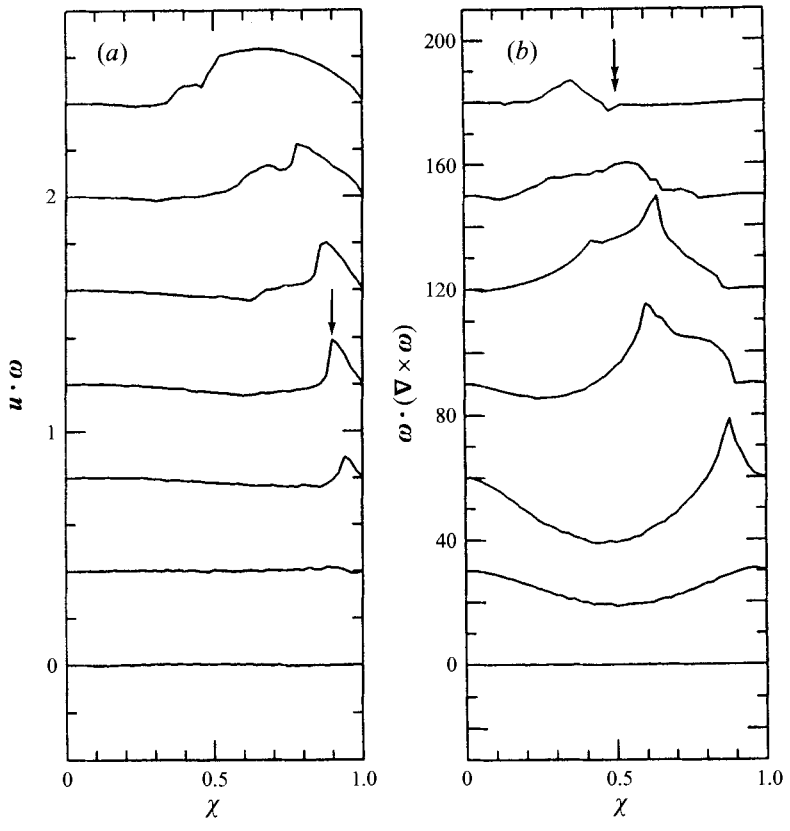

FIGURE 6. Time evolution of (*a*) the distribution of helicity and (*b*) helicity change for each vortex surface of run-5d, both of which are divided by the area to represent a density. The lines from bottom to top correspond to $t = 0$, 5, 10, 15, 20, 35, 50, respectively, and shifted upward to avoid overlapping.

where the rate of helicity change is almost negligible as shown by the double arrow in figure 6(*b*). So the field relaxes to the state where both nonlinear effects and helicity change will be negligibly small, which reminds us of the helical Beltrami state.

Lastly, it may be useful to show the difference between the distribution of helicity on each vortex surface and that of helicity density. The latter quantity has been used to investigate helicity dynamics in almost all numerical simulations, though the former one is superior from a theoretical view point. In figure 7, the distribution of helicity density $\boldsymbol{u} \cdot \boldsymbol{\omega}$ and the rate of helicity change $\boldsymbol{\omega} \cdot (\nabla \times \boldsymbol{\omega})$ at the initial instant are shown. Although the helicity on each vortex surface is zero, the helicity density is distributed with a relatively large organized structure. One should pay attention to the difference between them and take care in the discussion: if helicity density is zero everywhere, the helicity on the vortex surface is zero too, of course, but the reverse is not always the case.

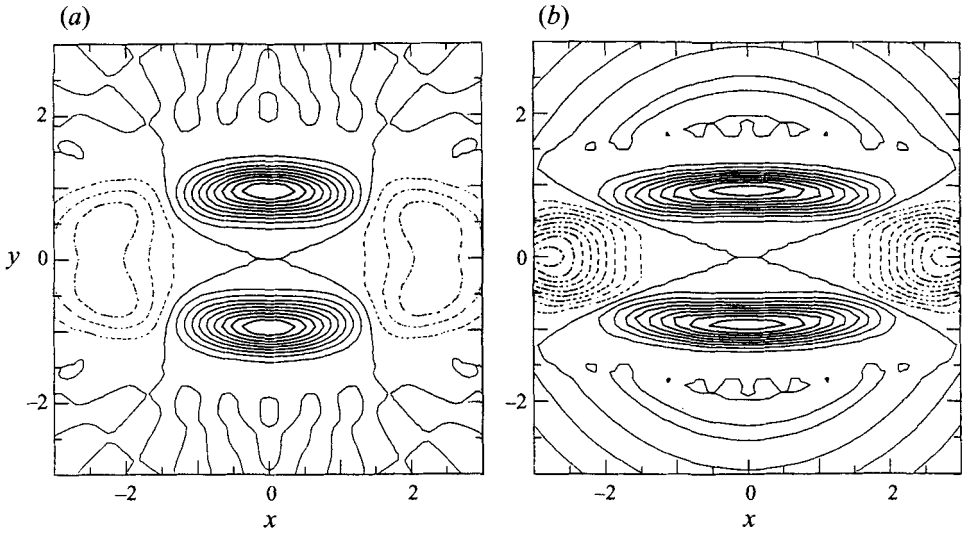

FIGURE 7. Distribution of (*a*) $\boldsymbol{u}\cdot\boldsymbol{\omega}$ and (*b*) $\boldsymbol{\omega}\cdot(\nabla\times\boldsymbol{\omega})$ at the initial instant for Case I. Solid lines and dashed lines respectively show positive and negative values for every 10% of each maximum value.

4.3. *Fourier spectrum of helicity*

Let us define the helicity spectrum in the same manner as the definition of Fourier spectrum in a usual two-dimensional flow as

$$\begin{aligned}\tilde{H}(k,t) &= \frac{1}{2\pi}\int_0^{2\pi} \mathrm{d}\phi_k \tilde{H}(k,\phi_k,t)\\ &= \frac{1}{2\pi}\int_0^{2\pi} \mathrm{d}\phi_k \left(\int_0^{2\pi}\mathrm{d}\phi\int_0^{\infty}\mathrm{d}r\,\boldsymbol{u}\cdot\boldsymbol{\omega}\,\mathrm{e}^{-\mathrm{i}kr\cos(\phi-\phi_k)}\right)\\ &= 2\pi\int_0^{\infty}\mathrm{d}r\,rh^2J_0(kr)\sum_n\left(-\frac{\mathrm{d}\psi_n}{\mathrm{d}r}\frac{\mathrm{d}\chi_n^*}{\mathrm{d}r}-\frac{2n^2}{r^2h^2}\psi_n\chi_n^*-2\epsilon h^2\chi_n\chi_n^*+\chi_n\varpi_n^*\right), \quad (4.1)\end{aligned}$$

where $J_n(kr)$ is the nth-order Bessel function of the first kind and use has been made of the expression (2.5) and the relation

$$\mathrm{e}^{-\mathrm{i}kr\cos(\phi-\phi_k)} = \sum_n(-\mathrm{i})^nJ_n(kr)\,\mathrm{e}^{-\mathrm{i}n(\phi-\phi_k)}. \quad (4.2)$$

Helicity is not a positive definite quantity, which is qualitatively different from energy and enstrophy. In figure 8, the time evolution of the helicity spectrum is shown, where an open circle represents a positive value and a black triangle a negative one. As the spiral structure of vorticity evolves, the Fourier components in higher-wavenumbers ranges are excited. It is interesting to note that the helicity spectra with either positive or negative sign are not randomly distributed but localized over finite-wavenumber intervals, and do not evolve in the same manner. The spectrum for positive helicity is transferred to larger length scales, while that for negative one is transferred to smaller length scales and dissipated by viscous effects (figure 8(*a–c*)). As a result, the positive ones assemble in small-wavenumber regions, and then positive total helicity emerges, or survives (figure 8*d–f*, see also figure 9). This process is a contrast to the one-way transfer of enstrophy.

Now, we briefly explain why and where the helicity takes the positive or negative

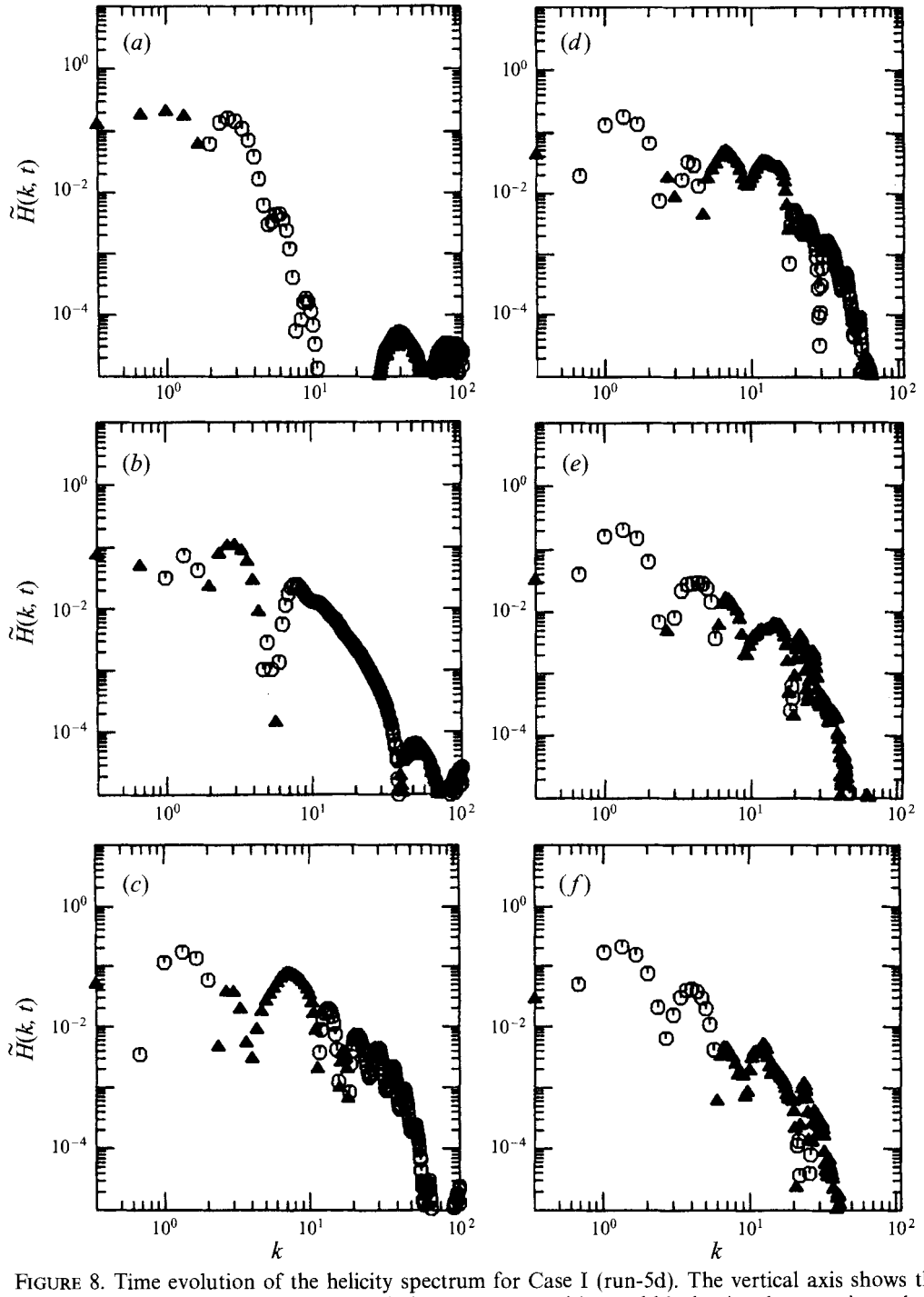

FIGURE 8. Time evolution of the helicity spectrum for Case I (run-5d). The vertical axis shows the absolute value of the amplitude; open circles represent positive and black triangles negative values. (*a*) $t = 0$, (*b*) $t = 5$, (*c*) $t = 10$, (*d*) $t = 15$, (*e*) $t = 35$, (*f*) $t = 50$.

sign in the previous results. Let us consider the helicity between two vortex surfaces, say the level lines with $\chi = \chi_1$ and $\chi = \chi_2$:

$$H_{[\chi_1:\chi_2]} = \int_{[\chi_1:\chi_2]} \boldsymbol{u}\cdot\boldsymbol{\omega}\, r\mathrm{d}r\mathrm{d}\phi$$
$$= -\int_{[\chi_1:\chi_2]} \left\{ \frac{\partial}{\partial r}\left(h^2 r \frac{\partial \psi}{\partial r}\chi\right) + \frac{1}{r}\frac{\partial}{\partial \phi}\left(\frac{\partial \psi}{\partial \phi}\chi\right) + 2h^2 r(\epsilon h^2 \chi + \varpi)\chi \right\} \mathrm{d}r\mathrm{d}\phi. \quad (4.3)$$

Using the initial condition (3.6), we can rewrite it as

$$H_{[\chi_1:\chi_2]} = \int_0^{2\pi} \left[-h^2 r \frac{\partial \psi}{\partial r}\chi + \epsilon h^2 r^2 \chi^2 \right]_{r_1(\phi)}^{r_2(\phi)} \mathrm{d}\phi \quad (4.4)$$

where r_i $(i = 1, 2)$ is defined as $\chi(r_i(\phi), \phi) = \chi_i$. At the initial instant, the first and second terms in (4.4) balance to give zero helicity for all $0 \leqslant \chi = \chi_i \leqslant 1$. And the second term is now positive definite because $0 < \epsilon = 1$. The helicity between the vortex surfaces becomes negative (positive) in the region where $\partial\psi/\partial r$ becomes larger (smaller). So that, roughly speaking, the helicity has a tendency to be negative (positive) in (outside) the region where the field has smaller (larger) length scale in the r-direction, such as the spiral structure (axisymmetric structure near origin) as shown in §4.2. This also explains why in Fourier space the positive helicity is transferred to the higher-wavenumber range and dissipated, while the negative helicity is transferred to the lower-wavenumber range and survives as shown in figure 8.

4.4. *Reynolds number dependence*

We have simulated the field for six values of viscosity. Their parameters are listed in table 1. In figure 9, we show the time variations of energy, enstrophy, helicity and rate of helicity change for these six simulations. One knows that the generated helicity, the change of the vortex structure, is a meaningful amount, since the circulation for the present initial condition is 1: $\Gamma_\phi = \int_0^\infty \omega_\phi \mathrm{d}r = 1$ for unit height in z, and therefore, the helicity corresponding to once-linked vortex filaments with this circulation is $2\Gamma_\phi^2 = 2$ (see Moffatt 1969). The evolution of total helicity is qualitatively similar to the result by Aref & Zawadzki (1991), who simulated two unlinked elliptical rings of vorticity initially in parallel planes. Helicity changes its sign from negative to positive. They did not consider this change of sign and the later stage in their paper. And the positive magnitude is larger than the negative magnitude, which is a contrast with their result. The negative stage is due to the vorticity reconnection of non-axisymmetry in an elliptical structure, i.e. the $2n$ $(n = 1,2,...)$ Fourier modes in the ϕ-direction. The continuous distribution of elliptical vorticity may play a central role in later stage. More of both positive and negative helicity is generated for smaller viscosity.

The enstrophy takes a peak value at some time, which is similar to that observed in general three-dimensional large-Reynolds-number flows starting from the field with large length scale. The viscous dependence of these peak values, however, is weaker than that of the three-dimensional case, and its dependence is nearly $Q_{\mathrm{peak}} \propto \nu^{-1/2}$. This is caused by the effect of vortex stretching which creates small-length-scale structures, now layers. This structure is different from a cudgel structure, sometimes called a worm or a sinew, observed in three-dimensional flows. A brief explanation of this mechanism is presented in the Appendix.

Comparing the time variations of energy and helicity, one sees that as the viscosity decreases, the energy is more conserved, whereas the variation of helicity becomes larger. This is because of the magnification of vorticity, vortex stretching, as discussed

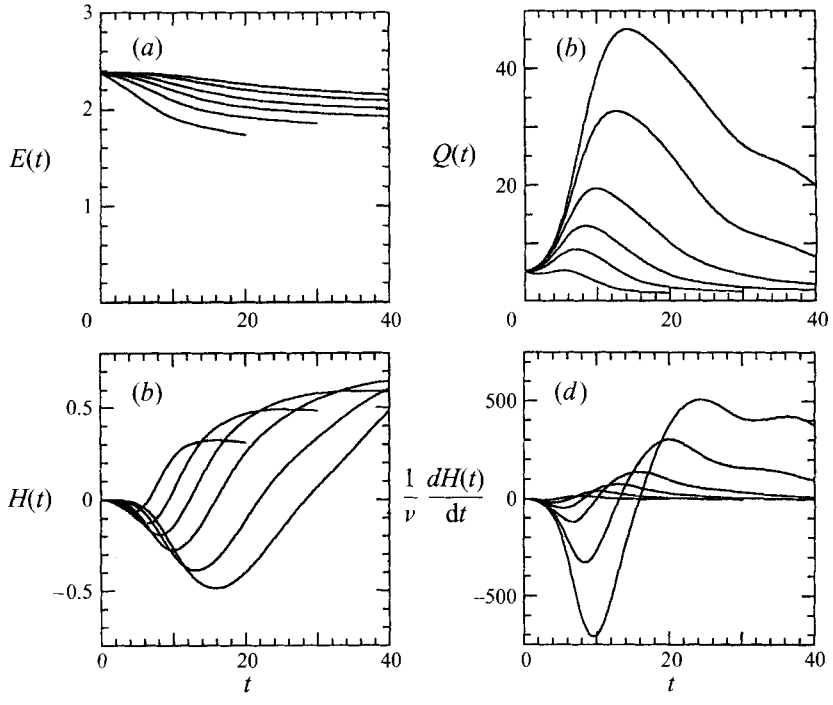

FIGURE 9. Time variation and viscous dependence of (*a*) energy, (*b*) enstrophy, (*c*) helicity and (*d*) rate of helicity change for Case I (run-1 – run-6).

in the preceding paragraph, though the contribution of the angle between the velocity and vorticity makes the problem more difficult. And for smaller viscosity the contact zones of vortex layers are more elongated, so that the stretched vorticity reconnects more actively. However this variation of helicity does not necessarily mean the breakdown of helicity invariance in the inviscid limit. More helicity is preserved for smaller viscosity when it is compared at a fixed time in the period before the peak, and the peak time also seems to be infinitely large in the inviscid limit.

5. Numerical results for Case II

In this section, we briefly summarize the numerical results obtained for Case II to compare with the results obtained for Case I. The initial flow field has the same equi-vorticity surfaces as those in Case I, but the vortex lines and the vortex surfaces are different (see figures 1, 2*a* and 10*a*). Equi-vorticity surfaces are elliptic in the (r, ϕ)-plane, but the vorticity surfaces are circular (r =const.) because $\chi = 0$.

5.1. *Vorticity dynamics*

The time evolution of the vortex lines is shown in figure 10 in the same manner as figure 2. Although the structure of the vortex lines is three-dimensional from the start, the elliptical high-vorticity regions are deformed into an S-shape and then into a spiral, which qualitatively resembles Case I. The mechanism for this deformation is different, since the z-component of vorticity and its circulation in the (x, y)-plane are not zero. It is similar to the generating mechanism of the spiral in vortex merging in a usual two-dimensional flow. The sign of the z-component of the vortex is positive everywhere for all time.

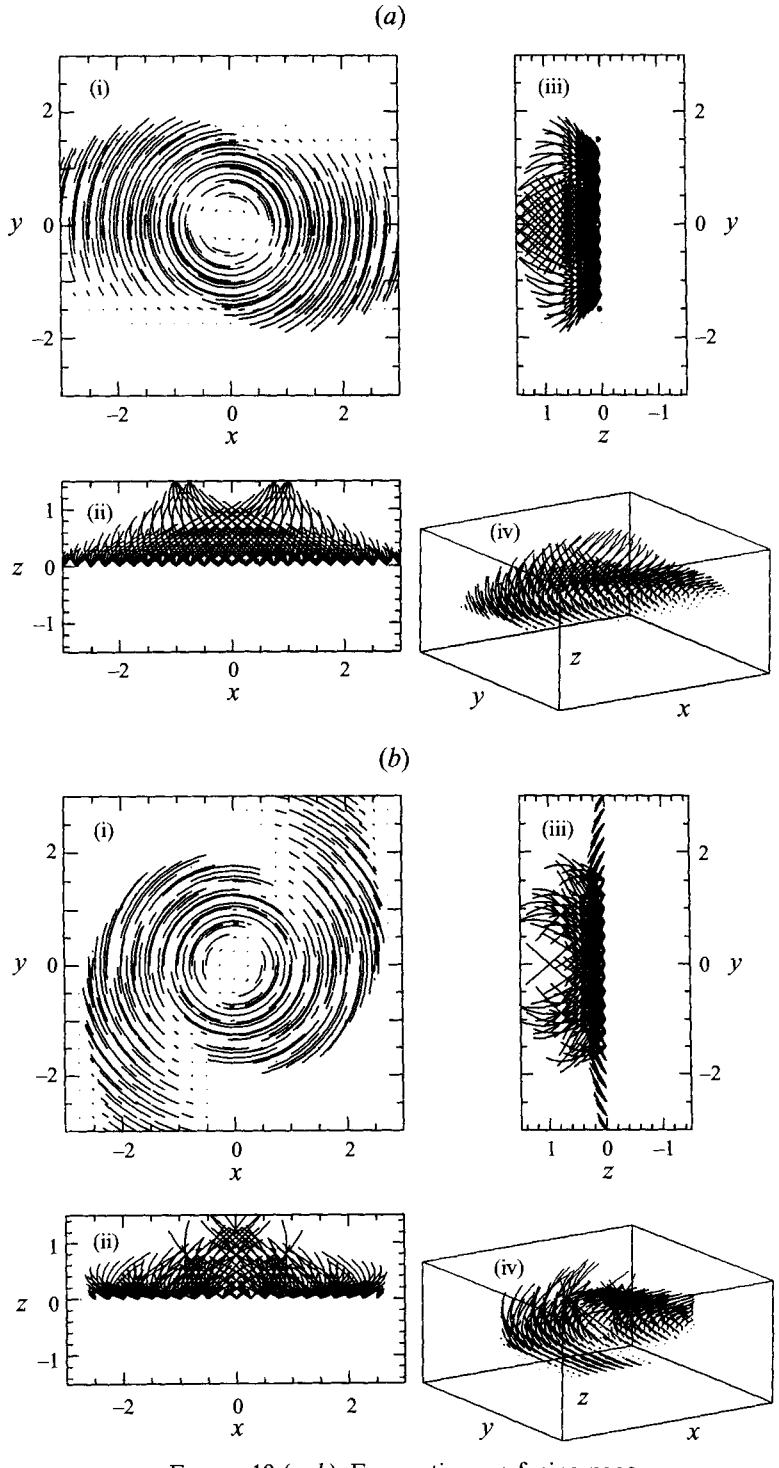

FIGURE 10 (*a*, *b*). For caption see facing page.

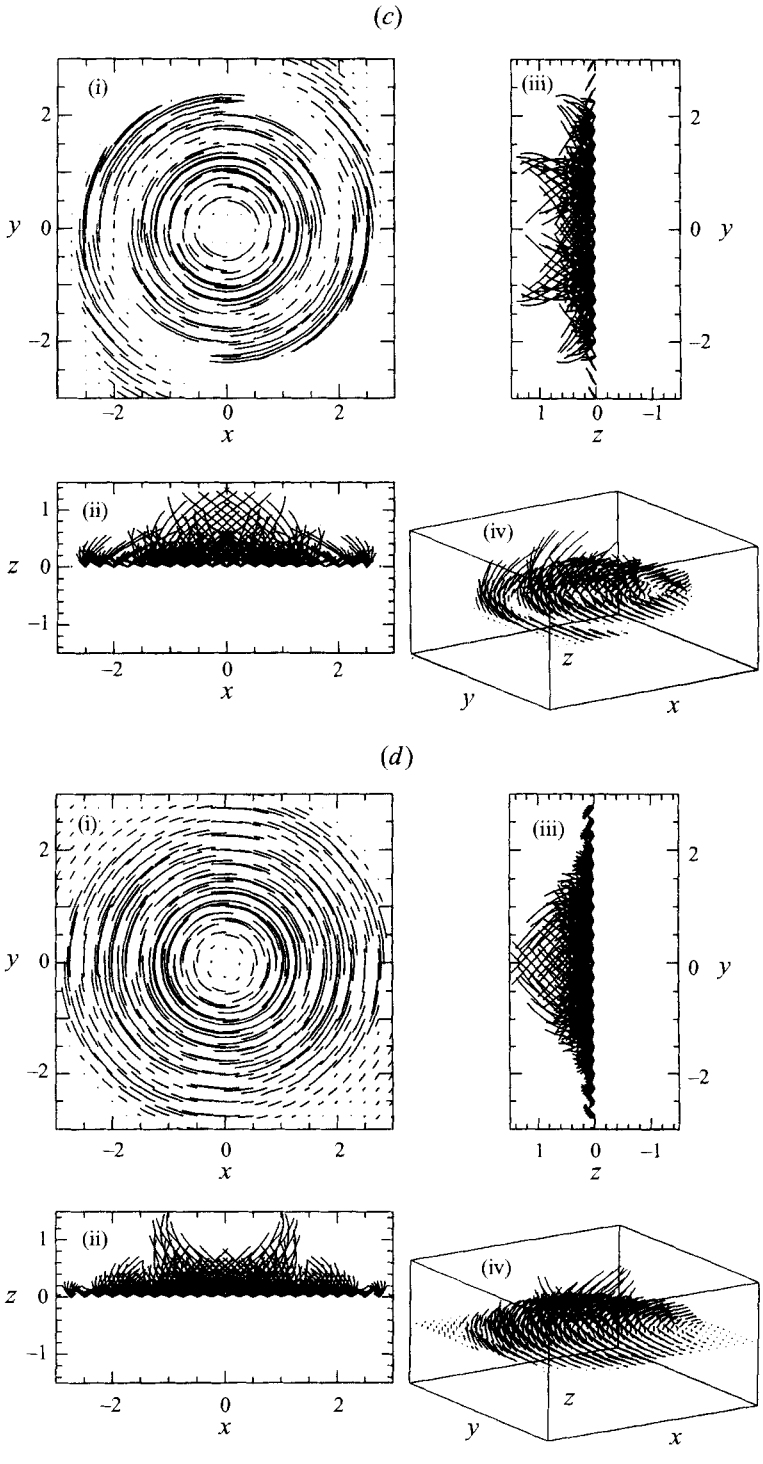

FIGURE 10. Time evolution of the vortex lines for Case II. $(N_r, N_\phi) = (256, 128)$ and $\nu = 0.0002$. (*a*) $t = 0$, (*b*) $t = 4$, (*c*) $t = 10$, (*d*) $t = 50$. See also the caption of figure 2.

The vortex lines relax to an axisymmetric helical state without experiencing the thin structure of vortex layers. One might think that the direction of this relaxed state seems to be opposite to that in Case I. Considering the invariance of the system under the transformation $(\chi, \psi, \phi) \rightarrow (-\chi, -\psi, -\phi)$, one knows that this relaxed state is similar to that in Case I. If our simulation is started with the initial condition obtained by changing the sign of (3.8), $\varpi \rightarrow -\varpi$, we obtain the same dynamics except for the signs of χ and ψ, that is $\boldsymbol{u}$ and ω. It should be noted that the sign of helicity is not changed under this transformation.

5.2. *Reynolds number dependence*

The enstrophy decays monotonically in time, in contrast with Case I, though the figures are omitted. The effect of vortex stretching is too weak to show the three-dimensional aspect. This may be related to the fact that the vorticity field is able to relax to an axisymmetric helical structure without topological change of vortex surfaces, since the vortex surfaces are axisymmetric from the start.

Moreover we can show that even if the fluid is inviscid ($\nu = 0$), the enstrophy does not increase when $\chi = 0$. First, if $\chi = 0$ at some time, χ remains zero following from equation (2.6) in the inviscid case because the stretching term in the vorticity equation is now $(\boldsymbol{\omega} \cdot \nabla)\boldsymbol{u} = (\varpi \boldsymbol{h} \cdot \nabla)\boldsymbol{u}$. Recalling the alternative definition of the helical symmetry (2.4), the right-hand side of the above equation is zero. In other words, we can say that there is no vortex stretching when $\chi = 0$. It should be noted that χ may be non-zero in a small but finite viscosity fluid, even if we start from the initial condition with $\chi = 0$. So the above argument is not straightforwardly applied to our case. But we know that the enstrophy for the viscous fluid is bounded from above by the value in the corresponding inviscid case when the field is smooth. We may conclude that the enstrophy in Case II decays monotonically even in much larger Reynolds number flows.

The helicity increases monotonically within the simulated period. (We have done a fairly long time simulation until $t \sim 10^4$.) It should be noted that in Case II the energy E_0 is infinite because of the non-zero total circulation of ω_z, although the enstrophy and helicity are the same as those in Case I at the initial time. The sign of the helicity is the same as that of the helicity in the later stage in Case I. The helical symmetry, $\epsilon > 0$, seems to prefer the axisymmetric helical structure with positive helicity as a relaxed state; a detailed analysis will be reported in a separate paper.

The smaller the viscosity is, the more both the energy and the helicity are conserved. So one may think that in the inviscid limit both quantities are preserved and the dynamics converges smoothly to that of Euler flow. There seems to be no singularity at all and also to be neither energy transfer nor helicity transfer in the high Reynolds number flow. Furthermore, the enstrophy is also more conserved for smaller viscosity, which reminds us of the conservation law in two-dimensional flow. The viscosity dependences of the enstrophy and the helicity at the same time are almost $\nu^{1/2}$ and ν respectively, although the fluctuations are relatively large. These facts tell us that the viscous length scale is almost proportional to $\nu^{1/2}$ on the average.

5.3. *Helicity in Fourier space*

We examine the generation process of helicity in Fourier space. It is quite different from that in Case I, as seen by comparing figures 11 and 8. Since both helicity and helicity density are zero at the initial instant in Case II, the Fourier components of all modes are also zero. The amplitudes of all modes grow in the same way with little change of their distribution. That is to say, the helicity is not transferred to

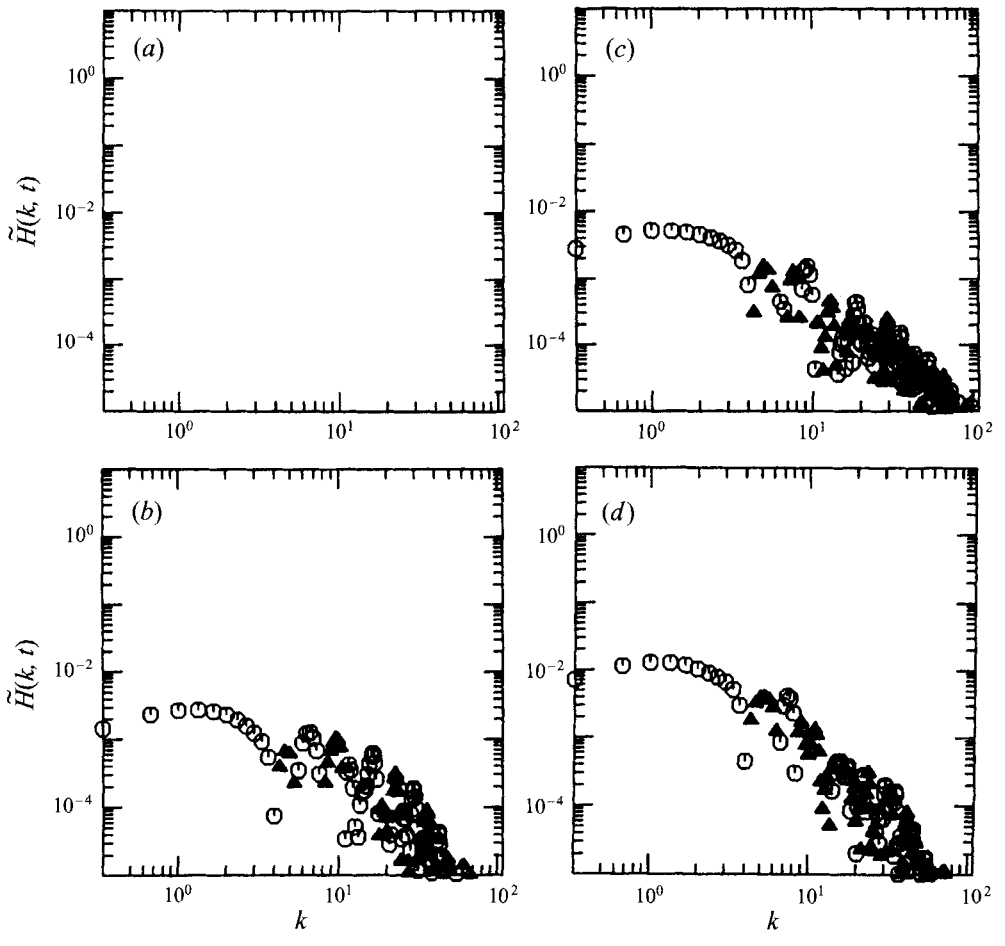

FIGURE 11. Time evolution of the helicity spectrum for Case II. $(N_r, N_\phi) = (256, 128), \nu = 0.0002$. (*a*) $t = 0$, (*b*) $t = 10$, (*c*) $t = 20$, (*d*) $t = 50$. See also the caption of figure 8 .

smaller or larger length scales, but the total helicity grows as a result of growth of Fourier amplitudes. This also shows that most vorticity distributions change only within r =const., axisymmetrically, since the spectrum is an r-directional spectrum integrated in the ϕ-direction. This evolution in Fourier space is consistent with the above result that vortex surfaces are not changed drastically but remained circular, and the vortex stretching is too weak to cause a thin vortex layer.

6. Summary and concluding remarks

We have simulated flow with helical symmetry and investigated mainly the generation of helicity and the vorticity dynamics. Both our initial conditions, Cases I and II, have zero helicity and a twisted elliptical tube structure of the high-vorticity region. According to the vortex stretching, roughly speaking, the characteristics of three-dimensional flows are observed in Case I, and those of two-dimensional flows in Case II. In the equi-vorticity presentation, the vortex structure in the (x, y)-plane evolves from elliptic to S-shaped, then to a spiral, and an axisymmetric helical structure in that order in both cases. But the structure and evolution of vortex surfaces and vortex lines are quite different from each other. During the evolution, helicity is

generated and energy is dissipated by viscous effects. In Case I, the generated total helicity changes its sign from negative to positive corresponding to the change of the vortex structure from S-shaped to an axisymmetric structure. On the other hand, the helicity gradually increases from zero monotonically in Case II.

Both total energy and total helicity are inviscid invariants, which restricts the dynamics and plays an important role in the turbulence theory. Not only the total helicity but also the helicity surrounded by arbitrary vortex surfaces are conserved in an inviscid fluid. Helicity dynamics in Fourier space for homogeneous three-dimensional turbulent flow was investigated by Waleffe (1992). He used 'helical decomposition' and made a detailed analysis of the triad interaction of each decomposed Fourier component. Some researchers after him have applied the helical decomposition to investigate the vorticity dynamics in real space. But each decomposed helicity part is not an inviscid invariant, though the total is.

To see the dynamics of helicity, we drew contour graphs of $\chi(r, \phi)$, which gives the vortex surfaces, and the time evolution of the density distribution of helicity over each vortex surface. Most helicity is generated in the spiral structure where the slope of χ is steep, that is the vortex surfaces accumulate densely. The generated helicity is located in an axisymmetric helical structure near the origin, which grows to occupy a larger circle with being little dissipated.

We also examined the time evolution of the Fourier spectrum of helicity, and found that there are at least two types of helicity generation processes. The helicity is transferred to smaller or larger length scales according to its sign, and the helicity transferred to smaller length scales is dissipated by viscous effects. Then the helicity with the other sign survives, which is the generation of (total) helicity as observed in Case I. The other type is helicity generation without changing the distribution so much in the Fourier space. The amplitude of each modes becomes larger, and so the total helicity also becomes larger as a result, as observed in Case II. This difference arising from initial condition is due to the thinning of structure by vortex stretching.

Vortex stretching is another distinctive feature in three-dimensional flows. We know this from the fact that the time evolution of enstrophy has a maximum. The viscous dependence of the peak value in Case I is nearly $\nu^{-1/2}$, which is a weaker dependence than that in three-dimensional flow.† On the other hand, there is no maximum in Case II.

In Case I, we found unexpected phenomena in the viscous dependence of helicity. As the viscosity becomes smaller, more energy is preserved. However, the helicity changes more violently and more is generated. This unexpected phenomenon is understood by the fact that the stretched vorticity reconnects more actively in a more elongated contact zone between vortex layers. It should be noted that this does not mean the breakdown of invariance of helicity in the inviscid limit, since the time scale also becomes larger.

The spiral is a key structure in investigating a (fractional) power-law spectrum of turbulent flow (Lundgren 1982; Moffatt 1984; Gilbert 1988) as well as the merging of two like-signed vortex patches. Even if the circulation in the z-direction is zero, we observed a spiral structure of vorticity in Case I. The Jacobian type of nonlinear term and the virtual azimuthal velocity, or the contribution from u_z, may help our understanding of the mechanism causing a spiral structure. On the other hand, the

† Recently I found the ν^{-1}-dependence in the numerical simulation of an isotropic three-dimensional turbulent flow. The same explanation as in the Appendix may also apply regarding a cudgel as a fundamental structure.

Fourier spectrum of enstrophy shows three kinds of power law as the spiral structure develops. Since these are transient and sufficient interpretation has not been done yet, we will omit a discussion about it here.

Because helicity is also related to the topology of vortex lines, it is sometimes referred to in the discussion of vorticity reconnection. Kida & Takaoka (1991, 1994) recently pointed out the importance of tracking of vortex surfaces (vortex lines) and the difficulty in quantifying vorticity reconnection. The present symmetry has the advantage in investigating these problems of the easiness in constructing vortex surfaces, though this has not been discussed at length yet. It is also still unresolved whether the relaxed state with axisymmetric helical structure emerging for both initial conditions is unique in the helically symmetric flow.

I would like to acknowledge Professors Kakutani and Kida for reading the manuscript. Numerical computation has been done on FACOM-VP2600 in Kyoto University Data Processing Center. This work was partially supported by a Grant-in-Aid for Scientific Research from the Ministry of Education, Science and Culture of Japan.

Appendix. Viscosity dependence of Q_{peak}

The viscosity dependence of the peak value of enstrophy, $Q_{\mathrm{peak}} \propto \nu^{-1/2}$, reminds us of the similar dependence of the peak value of the palinstrophy in the early period of the simulation of two-dimensional turbulence in an incompressible fluid (Kida *et al.* 1988). In the both fields, typical structures are layers and both integrated quantities showing peaks are proportional to the time-derivative of inviscid conserved quantities divided by viscosity. One possible explanation of this viscous dependence is given by Kida, Yamada & Ohkitani (1988). In our case, the energy, the inviscid conserved quantity, at the peak time is slightly larger for smaller viscosity. This leads us to question their assumption that the area of active field is proportional to the thickness of vortex layer, that is, $\nu^{1/2}$.

We propose here another possible explanation for the viscosity dependence. The averaged thickness of the vortex layers is estimated to be proportional to $\nu^{1/2}$ as in the discussion by Kida *et al.* (see also the last paragraph in §5.2). The wall of an initial twisted elliptical tube of high vorticity is stretched to become a layer, whose height and length are estimated to be proportional to ν^0 and $\nu^{-1/2}$ respectively, because of the incompressibility of the fluid and the fixed pitch in the z-direction. Therefore neglecting slight viscous dissipation, we estimate that the vorticity whose direction is almost that of the layer is magnified by between ν^0 and $\nu^{-1/2}$ according to its direction. The peak value of enstrophy, then, is proportional to between ν^0 and ν^{-1}, since the volume (area) of the active field is assumed to be preserved now.

The eigenvalues of the rate of strain tensor $\boldsymbol{S}$ are $\lambda, -\lambda$ and 0. The eigenvector with zero eigenvalue is in the $\boldsymbol{h}$-direction. The enstrophy is produced through vortex stretching, $\boldsymbol{\omega S \omega}$. Now it should be noted that the vortex structure, a layer, does *not* always turn to the stretching direction. Let us consider the lump of vorticity advected passively by the (linear) shear flow $\boldsymbol{U}$ as an example, e.g. $\boldsymbol{U} = (Cy, 0, 0)$. Though the directions of greatest stretching and compressing of the rate of strain tensor are inclined 45° up and down from the direction of velocity respectively, $\boldsymbol{e}_x \pm \boldsymbol{e}_y$, the vortex structure is elongated and is turned to the direction of the velocity, $\boldsymbol{e}_x$.

The viscosity dependence of the peak value of the enstrophy depends on the type of dominant flow. If there is no vortex stretching in the field as in Case II,

which corresponds to the ν^0 case of the viscosity dependence of the peak value, the enstrophy decreases monotonically and is more preserved for smaller viscosity. If the straining flow dominates the field as examined by Takaoka (1990, 1991), where the direction of vortex structure and the stretching direction coincide, the peak value of enstrophy is proportional to ν^{-1}. Because the rate of strain tensor is now diagonal, the enstrophy production by vortex stretching is proportional to $\omega_\alpha\omega_\alpha$, which has a $(\nu^{-1/2})^2 = \nu^{-1}$ dependence in the stretching direction. This was shown analytically for both the peak value of enstrophy in three-dimensional flow and the peak value of palinstrophy in two-dimensional flow (Takaoka 1990, 1991). And if the shear flow dominates the field as in Case I, the vortex structure is elongated in the maximum stretching direction initially and is turned towards the stream direction, the neutrally stretching direction. Vorticity might experience averaged stretching $\nu^{-1/4}$ in this case, so that the peak value of the enstrophy is proportional to $\nu^{-1/2}$. Because the rate of strain tensor is off-diagonal in the (local) coordinate parallel to the velocity, the enstrophy production by vortex stretching is now proportional to $\omega_\alpha\omega_\beta$ which is at most $\nu^{-1/2}\nu^0 = \nu^{-1/2}$.

REFERENCES

AREF, H. & ZAWADZKI, I. 1991 Linking of vortex ring. *Nature* **354**, 50–53.

BUNTINE, J. D. & PULLIN, D. I. 1989 Merger and cancellation of strained vortices. *J. Fluid Mech.* **205**, 263–295.

DRITSCHEL, D. G. 1991 Generalized helical Beltrami flows in hydrodynamics and magneto hydrodynamics. *J. Fluid Mech.* **222**, 525–541.

FRISCH, U., SHE, Z. S. & SULEM, P. L. 1987 Large-scale flow driven by the anisotropic kinetic alpha effect. *Physica* D **28**, 382–392.

GILBERT, A. D. 1988 Spiral structures and spectra in two-dimensional turbulence. *J. Fluid Mech.* **193**, 475–497.

GRAUER, R. & SIDERIS, T. C. 1991 Numerical computation of 3-D incompressible ideal fluids with swirl. *Phys. Rev. Lett.* **67**, 3511–3514.

KELVIN, LORD 1880 Vibrations of a columnar vortex. *Phil. Mag.* **10**, 155–168.

KIDA, S. & TAKAOKA, M. 1987 Bridging in vortex reconnection. *Phys. Fluids* **30**, 2911–2924.

KIDA, S. & TAKAOKA, M. 1988 Reconnection of vortex tubes. *Fluid Dyn. Res.* **3**, 257–261.

KIDA, S. & TAKAOKA, M. 1991 Breakdown of frozen motion and vorticity reconnection. *J. Phys. Soc. Japan* **60**, 2184–2196.

KIDA, S. & TAKAOKA, M. 1994 Vortex reconnection. *Ann. Rev. Fluid Mech.* **26**, 169–189.

KIDA, S., TAKAOKA, M. & HUSSAIN, F. 1991 Collision of two vortex rings. *J. Fluid Mech.* **230**, 583–646.

KIDA, S., YAMADA, M. & OHKITANI, K. 1988 The energy spectrum in the universal range of two-dimensional turbulence. *Fluid Dyn. Res.* **4**, 271–301.

KRAUSE, F. & RUDIGER, G. 1974 On the Reynolds stresses in mean-field hydrodynamics. *Astron. Nachr.* **295**, 93–99.

LANDMAN, M. J. 1990*a* Time-dependent helical waves in rotating pipe flow. *J. Fluid Mech.* **221**, 289–310.

LANDMAN, M. J. 1990*b* On the generation of helical waves in circular pipe flow. *Phys. Fluids* A **2**, 738–747.

LUNDGREN, T. S. 1982 Strained spiral vortex model for turbulent fine structure. *Phys. Fluids* **25**, 2193–2203.

MAHALOV, A., TITI, E. S. & LEIBOVICH, S. 1990 Invariant helical subspaces for the Navier–Stokes equations. *Arch. Rat. Mech. Anal.* **112**, 193–222.

MELANDER, M. V., ZABUSKY, N. J. & MCWILLIAMS, J. C. 1988 Symmetric vortex merger in two dimensions: causes and conditions. *J. Fluid Mech.* **195**, 303–340.

MOFFATT, H. K. 1969 The degree of knottedness of tangled vortex lines. *J. Fluid Mech.* **159**, 117–129.

MOFFATT, H. K. 1984 Simple topological aspects of turbulent vorticity dynamics. *In Proc. IUTAM Symp. on Turbulence and Chaotic Phenomena in Fluids* (ed. T. Tastumi), pp. 223–230. Elsevier.

MOFFATT, H. K. & RICCA, R. L. 1992 Helicity and the Călugăreanu Invariant. *Proc. R. Soc. Lond.* A **439**, 411–429.

MOFFATT, H. K. & TSINOBER, A. 1992 Helicity in laminar and turbulent flow. *Ann. Rev. Fluid Mech.* **24**, 281–312.

PUMIR, A. & SIGGIA, E. 1992 Finite-time singularities in the axisymmetric three-dimensional Euler equations. *Phys. Rev. Lett.* **68**, 1511–1514.

TAKAOKA, M. 1990 Some characteristics of exact strained solutions to the two dimensional Navier–Stokes equation. *J. Phys. Soc. Japan* **59**, 2365–2373.

TAKAOKA, M. 1991 Straining effects and vortex reconnection of solutions to the 3-D Navier–Stokes equation. *J. Phys. Soc. Japan* **60**, 2602–2612.

TUR, A. V. & YANOVSKY, V. V. 1993 Invariants in dissipationless hydrodynamic media. *J. Fluid Mech.* **248**, 67–106.

WALEFFE, F. 1992 The nature of triad interactions in homogeneous turbulence. *Phys. Fluids* A **4**, 350–363.